Forum

Light-to-Chemical Energy Conversion in Lamellar Solids and Thin Films

Paul G. Hoertz and Thomas E. Mallouk*

*Department of Chemistry, The Pennsylvania State University,
University Park, Pennsylvania 16802*

Photocatalytic water splitting by visible light is one of the most difficult and persistent challenges in chemistry. This Forum Article reviews progress in this field, focusing on efforts made in our laboratory to control electron- and energy-transfer reactions, and catalytic hydrogen and oxygen evolution, in lamellar solids and thin films.

Introduction

As the cost and environmental impact of fossil fuels continues to rise, the development of new strategies for converting sunlight to chemical energy has become an increasingly compelling problem for chemists. The photolysis of water could potentially produce stored chemical energy in the form of clean hydrogen from an abundant, renewable resource. Photoassisted water electrolysis using ultraviolet (UV) light was demonstrated over 30 years ago by Fujishima and Honda,[1] and more recently oxide photocatalysts for efficient overall water splitting by UV light have been discovered.[2] However, photochemical water splitting by *visible* light, which was described a decade ago as one of the "holy grails" of chemistry,[3] remains a difficult challenge today.

A generic artificial photosynthetic system is sketched in Scheme 1. Rapid energy transfer between antenna molecules funnels excitation to a photoredox center, which pumps electrons from the donor to the acceptor side of a chain of redox molecules. The sensitizer box may consist of an individual molecule, a semiconductor particle, or a dye-sensitized semiconductor particle. At the ends of this chain, catalytic reactions occur so that the transiently stored energy of an electron−hole pair is permanently stored in energetic chemical products. Although very many molecular and supramolecular systems have been created to carry out parts

Scheme 1. Artificial Photosynthesis
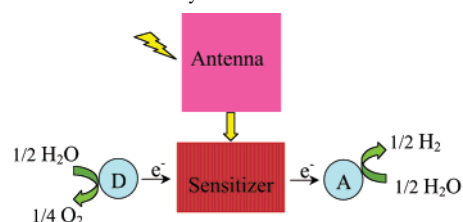
of this overall reaction scheme, so far there are very few examples (outside of natural photosynthesis) of visible-light-driven chemical transformations that store useful amounts of free energy.

This Forum Article discusses our efforts to design and construct hybrid organic−inorganic photosystems that attack this problem at several levels. We seek first to develop lamellar solids, redox assemblies in porous solids, and ordered thin films that position molecules in a vectorial fashion, with the precision needed to control energy- and electron-transfer rates. These molecules absorb visible light and transfer excitation energy and electrons, resulting in long-lived (microsecond to millisecond) charge separation. By coupling one end of the photoredox chain to nanoparticle catalysts, we have demonstrated photochemical hydrogen evolution from nonsacrificial electron donors, as well as efficient oxygen evolution in sacrificial systems. The remaining major challenge is to couple both ends of the photoredox chains to catalysts that can turn over faster than back electron transfer occurs. Possible routes to such systems are described at the conclusion of this Forum Article.

Thermodynamically, the water-splitting reaction (1) is uphill by 1.23 V and should, in principle, be readily accomplished by using visible light and an appropriate

(1) Fujishima, A.; Honda, K. *Nature* **1972**, *238*, 37−38.
(2) (a) Kato, H.; Kudo, A. *J. Phys. Chem. B* **2001**, *105*, 4285−4292. (b) Kato, H.; Asakura, K.; Kudo, A. *J. Am. Chem. Soc.* **2003**, *125*, 3082−3089.
(3) Bard, A. J.; Fox, M. A. *Acc. Chem. Res.* **1995**, *28*, 141−145.

photocatalyst. The thermodynamics of photocatalysis have been considered in detail by Bolton et al., who concluded that the overall water splitting at 10−15% energy conversion efficiency (assuming a quantum efficiency of 100% and a single-band-gap absorber)

$$2H_2O(l) \xrightarrow{n\ h\nu} 2H_2(g) + O_2(g) \qquad (1)$$
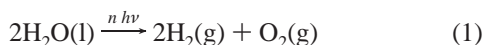
should be achievable with molecules or semiconductors that absorb light between 550 and 775 nm (2.25−1.60 eV). In practice, only a few visible light photocatalysts for water splitting have been discovered.[4,5] In no case does the overall quantum yield exceed 1%, meaning that the energy conversion efficiency is well below 0.1%. All of these systems employ relatively simple materials, such as doped oxide semiconductors or semiconductors coupled to oxide catalysts. The poor conversion efficiency of photocatalytic systems stands in sharp contrast to that of photoelectrochemical systems, in which water splitting has been reported with power conversion efficiencies as high as 18%.[6]

Important questions to ask in the design of visible-light water-splitting photocatalysts are, why is the quantum efficiency of the current systems so poor and what is needed to increase it to the level of semiconductor photoelectrochemical systems, which are typically 50−90%? The answer may be found by examining the results of studies on hydrogen- and oxygen-evolving half-cell photosystems, or so-called *sacrificial* photosystems. In these cases, the sensitizer in Scheme 1 is coupled to an electron relay and catalyst in only one direction, to produce hydrogen or oxygen. The photogenerated electron or hole on the sensitizer is removed irreversibly by a sacrificial acceptor or donor, respectively, which rapidly decomposes to products that do not interfere with the photocatalytic half-reaction. Typical sacrificial donors are reducing agents such as ethylenediaminetetraacetic acid or triethanolamine, whereas sacrificial acceptors are oxidizing agents such as persulfate. In cases where the excited state of the sensitizer is quenched by electron transfer to/from the sacrificial reagent, the quantum yield for hydrogen or oxygen evolution can be quite high (40−70%).[7,8] The high yields attained in sacrificial systems suggest that the essential *components* we have for water splitting (photosensitizers, electron relays, and colloidal catalysts) are already adequate for the job, at least at the proof-of-concept level. The failure of chemists to join the two half-reactions successfully for an overall water splitting has to do not with the components themselves but with short circuits between them. For example, methylviologen, a commonly used electron-acceptor relay, is rapidly reoxidized by molecular oxygen. Colloidal platinum, which is the most commonly used hydrogen evolution catalyst, is also an excellent catalyst for the recombination of hydrogen and oxygen to produce water [the reverse of reaction (1)].

It follows that successful photosystems must maintain sensitizers, electron relays, and catalysts in the proper spatial arrangement and chemical environment to prevent these recombination reactions. In natural photosystems, this is taken care of by the protein scaffolding that prevents contact between the wrong redox partners, by catalysts that are not good catalysts for reverse reactions (such as the reaction of oxygen with sugars), and by spatial compartmentalization of products. These natural assemblies are good examples of integrated chemical systems[9] that function through an interlocking sequence of electron transfer and catalytic reactions. Our research efforts over the past 15 years, which are summarized below, have focused primarily on the development of material synthetic techniques to address the problem of spatial organization in artifical integrated chemical systems.

Layer-by-Layer (LBL) Construction of Photoredox Assemblies

If one thinks of the problem of organizing photoredox molecules and catalysts into a linear chain, a lamellar arrangement (in which the components reside in an appropriate sequence of layers) provides the necessary spatial control, at least in the stacking direction. Early proof-of-concept experiments by Kuhn and Moebius[10] illustrated this idea with Langmuir−Blodgett thin films. These studies also provided some of the first reliable measurements of the distance dependence of outer-sphere electron-transfer reactions. However, Langmuir−Blodgett films are metastable and are not sufficiently robust for photocatalysis. Lamellar coordination solids and intercalation compounds are more rugged candidate materials for such assemblies, provided they can be grown with the appropriate sequence of layers.

Metal Phosphonates. Metal phosphonates are coordination solids that often crystallize as lamellar materials, with a morphology resembling pillared clays.[11] We recognized in 1988 the structural resemblance between the alternating organic−inorganic layers in these compounds and in Langmuir−Blodgett films and performed experiments to see if these materials could be grown one layer at a time on solid surfaces.[12] This strategy was based on the earlier work of Netzer and Sagiv, who built up thin films of organosilanes by a sequence of alternating adsorption and activation reactions.[13] In the case of metal phosphonates, thin film deposition was accomplished by alternately dipping a phos-

(4) Zou, Z.; Ye, J.; Sayama, K.; Arakawa, H. *Nature* **2001**, *414*, 625.

(5) Sayama, K.; Musaka, K.; Abe, R.; Abe, Y.; Arakawa, H. *Chem. Commun.* **2001**, 2416−2417.

(6) Khaselev, O.; Turner, J. A. *Science* **1998**, *280*, 425.

(7) Goldsmith, J. I.; Hudson, W. R.; Lowry, M. S.; Anderson, T. H.; Bernhard, S. *J. Am. Chem. Soc.* **2005**, *127*, ASAP article.

(8) Harriman, A.; Richoux, M.; Christensen, P. A.; Moseri, S.; Neta, P. *J. Chem. Soc., Faraday Trans. 1* **1987**, *83*, 3001.

(9) Bard, A. J. *Integrated Chemical Systems*; John Wiley and Sons: New York, 1994; pp 227−288.

(10) (a) Buecher, H.; Kuhn, H.; Mann, B.; Moebius, D.; Von Szentpaly, L.; Tillmann, P. *Photo. Sci. Eng.* **1967**, *11*, 233. (b) Kuhn, H.; Moebius, D. *Angew. Chem., Int. Ed. Engl.* **1971**, *10*, 620−37. (c) Polymeropoulos, E. E.; Moebius, D.; Kuhn, H. *J. Chem. Phys.* **1978**, *68*, 3918. (d) Kuhn, H. *Pure Appl. Chem.* **1981**, *53*, 2105.

(11) (a) Dines, M. B.; Griffith, P. C. *Inorg. Chem.* **1982**, *86*, 571. (b) Clearfield, A. J. *Mol. Catal.* **1984**, *27*, 251. (c) Alberti, G.; Costantino, U.; Kornyei, J.; Giovagnotti, M. L.; Luciani, *React. Polym., Ion Exch., Sorbents* **1985**, *4*, 1−10.

(12) Lee, H.; Kepley, L. J.; Hong, H.-G.; Mallouk, T. E. *J. Am. Chem. Soc.* **1988**, *110*, 618−620.

(13) Netzer, L.; Sagiv, J. *J. Am. Chem. Soc.* **1983**, *105*, 674−676.
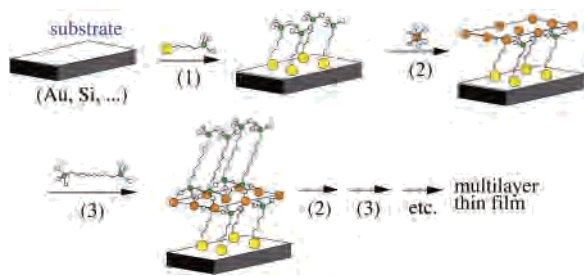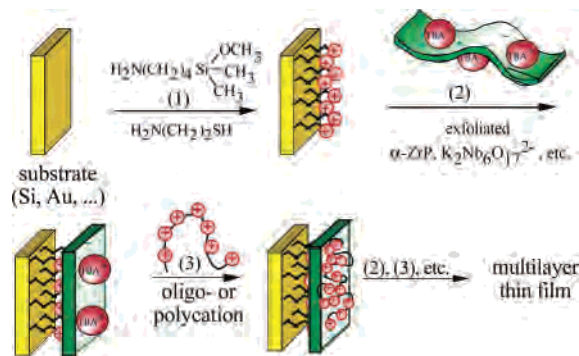
Figure 1. LBL adsorption of metal ions and bis(phosphonic acid)s to make a multilayer thin film. Yellow circles represent surface-active groups, e.g., thiol for Au or trimethoxysilyl for Si/SiO_x. Orange circles represent di-, tri-, or tetravalent metal ions. Small green circles represent phosphorus atoms.

Figure 2. LBL growth of polyanion/polycation films from lamellar colloids.

phonate-primed substrate in solutions of di-, tri-, or tetravalent metal salts and alkyl- or arylbis(phosphonic acid).[14] The same kind of sequential adsorption procedure (illustrated schematically in Figure 1) was subsequently developed for LBL growth of intercalated metal phosphates,[15] organic polyelectrolytes,[16] and coordination compounds[17] as ordered thin films.

Metal phosphonate films were subsequently characterized by several research groups. Thompson and co-workers used atomic force microscopy to study the dynamics of the assembly process and determined that phosphonate layers grew rapidly on Zr-terminated surfaces and then ripened more slowly to form very flat layers.[18] We determined that more rapid formation of well-ordered films (as determined by reflectance IR spectra) could be achieved with metal ions of lower charge, such as Cu^{2+} or Zn^{2+}.[19] Page et al. used X-ray reflectometry to compare the packing density of alkyl chains in hafnium phosphonate multilayers to that of the corresponding crystalline bulk solids.[20] Talham and co-workers devised a combined Langmuir−Blodgett/metal phosphonate adsorption method that gave particularly well-ordered LBL films of tetra- and divalent metal phosphonates.[21]

Photoinduced charge transfer in zirconium phosphonate LBL films was first studied by Katz et al., who made multilayer films consisting of 5,10,15,20-tetrakis(4-phosphonophenyl)porphyrin and N,N′-bis(3-phosphonopropyl)-4,4′-bipyridinium molecules interleaved by Zr^{4+} layers.[22] In the absence of the bipyridinium electron acceptor, the free base

porphyrin excited state decays with a fluorescence lifetime of 4 ns. Electron transfer from the porphyrin to the bipyridinium in adjacent layers was found to be competitive with singlet excited-state decay, as evidenced by a 60% loss in fluorescence intensity. Because of the ease with which layers of different sequences could be grown, Katz and co-workers were able to study different donor−acceptor sequences that also contained electroinactive alkanediyl bisphosphonate spacer layers. However, they were not able to observe the products of the electron-transfer reaction directly, so they could not comment on the effect of the lamellar structure in preventing back electron transfer.

Insulating and Semiconducting Sheets. The metal phosphonate assembly process is somewhat limiting because it requires that electron donors, acceptors, and sensitzers be derivatized with phosphonate groups. Following the discovery of the polyelectrolyte sequential adsorption process by Decher,[26] LBL assemblies were constructed by sequentially depositing two-dimensional inorganic, polyanionic sheets interleaved with polycationic layers.[23,24] These electrostatically assembled thin films were able to accommodate photoredox molecules bound to polyelectrolytes, as well as monomeric molecules such as porphyrins with sufficiently high positive or negative charge. Keller et al. demonstrated this idea by using anionic α-$Zr(HPO_4)_2$ (α-ZrP) sheets along with a cationic oligomer (Keggin ions, $[Al_{13}O_4(OH)_{24}(H_2O)_{12}]^{7+}$, or the protein, cytochrome c) or cationic polymer [poly(allylamine) hydrochloride, PAH].[24] Inorganic sheets were obtained by exfoliation of α-ZrP with tetrabutylammonium hydroxide (TBA^+OH^-) to create a suspension. In this particular case, exfoliation involves a two-step mechanism: (1) intercalation of TBA^+ cations between α-ZrP layers upon deprotonation, forming the intermediate $Zr(HPO_4)_{1.5}(TBA^+ PO_4^-)_{0.5}$ and expanding the interlayer spacing from 7.6 to 16.8 Å, and (2) further deprotonation causing delamination of the layers and subsequent formation of colloidal anionic sheets. The sequence of layer deposition steps utilized to grow films is shown schematically in Figure 2. The film thickness, as determined by ellipsometry, increased linearly with the number of α-ZrP/cation layers,

(14) Cao, G.; Hong, H.-G.; Mallouk, T. E. *Acc. Chem. Res.* **1992**, *25*, 420−427.
(15) (a) Rong, D.; Kim, Y. I.; Hong, H. G.; Krueger, J. S.; Mayer, J. E.; Mallouk, T. E. *Coord. Chem. Rev.* **1990**, *97*, 237−248.
(16) Decher, G.; Hong, J.-D. *Ber. Bunsen-Ges. Phys. Chem.* **1991**, *95*, 1430.
(17) (a) Evans, S. D.; Ulman, A.; Goppert-Berarducci, K. E.; Gerenser, L. J. *J. Am. Chem. Soc.* **1991**, *113*, 5866−5968. (b) Bell, C. M.; Arendt, M. F.; Gomez, L.; Schmehl, R. H.; Mallouk, T. E. *J. Am. Chem. Soc.* **1994**, *116*, 8374−8375.
(18) Byrd, H.; Snover, J. L.; Thompson, M. E. *Langmuir* **1995**, *11*, 4449.
(19) Yang, H. C.; Aoki, K.; Hong, H. G.; Sackett, D. D.; Arendt, M. F.; Yau, S. L.; Bell, C. M.; Mallouk, T. E. *J. Am. Chem. Soc.* **1993**, *115*, 11855−11862.
(20) Zeppenfeld, A. C.; Fiddler, S. L.; Ham, W. K.; Klopfenstein, B. J.; Page, C. J. *J. Am. Chem. Soc.* **1994**, *116*, 9158−9165.
(21) (a) Byrd, H.; Whipps, S.; Pike, J. K.; Nagler, S. E.; Talham, D. R. *J. Am. Chem. Soc.* **1994**, *116*, 295−301. (b) Byrd, H.; Pike, J. K.; Talham, D. R. *J. Am. Chem. Soc.* **1994**, *116*, 7903−7904.
(22) Ungashe, S. B.; Wilson, W. L.; Katz, H. E.; Scheller, G. R.; Putvinski, T. M. *J. Am. Chem. Soc.* **1992**, *114*, 8717.
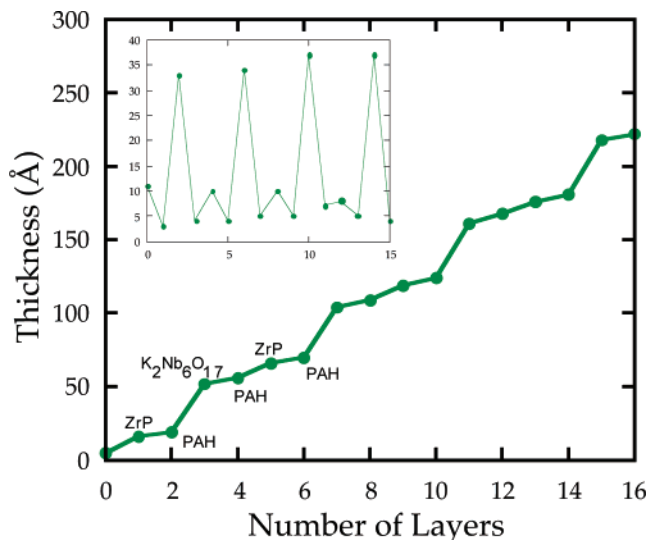(23) Kleinfeld, E. R.; Ferguson, G. S. *Science* **1994**, *265*, 370.
(24) (a) Keller, S. W.; Kim, H. N.; Mallouk, T. E. *J. Am. Chem. Soc.* **1994**, *116*, 8817. (b) Kim, H. N.; Keller, S. W.; Mallouk, T. E.; Schmitt, J.; Decher, G. *Chem. Mater.* **1997**, *9*, 1414.

or bilayers. From linear fits of the data, the thickness of each α-ZrP/cation bilayer was determined to be 13, 31, and 16 Å for α-ZrP/PAH, α-ZrP/cyt *c*, and α-ZrP/Al$_{13}$$^{7+}$, respectively. The bilayer thicknesses were in good agreement with the sum of the known α-ZrP layer spacing (7.6 Å)[25] and either the thickness of a single uncoiled PAH layer (5 Å)[26−34] or the crystallographic diameters of the oligocations.[35,36]

Layered metal oxide semiconductors (LMOSs) such as K$_4$-Nb$_6$O$_{17}$ and CsTi$_2$NbO$_7$ can also be used in place of α-ZrP. These quasi-2D semiconductors are of special interest for constructing electron-transfer assemblies because they can be sensitized with carboxylate- or phosphonate-derivatized dye molecules. Anionic LMOS sheets can be obtained by acid exchange followed by exfoliation with TBA$^+$OH$^-$. Sheets of K$_4$Nb$_6$O$_{17}$ contain two distinct interstitial sites for potassium cations; hence, after sequential treatment with a mild acid and TBA$^+$OH$^-$, the colloid exists as two niobate sheets sandwiching a layer of K$^+$. Ellipsometric measurements of LMOS/PAH films showed that the hexaniobate layers were 26 Å thick, consistent with the deposition of niobate−K$^+$−niobate sandwiches. In contrast, CsTi$_2$NbO$_7$ layers were only 16 Å thick, consistent with single-layer deposition for every LMOS cycle.

Because electrostatic interactions are the driving force for LBL film growth, the cationic and anionic layers can be easily substituted, creating the potential for a library of different heterostructures that vary in complexity. As a proof of this concept, Keller et al. alternated α-ZrP and K$_4$Nb$_6$O$_{17}$ anionic sheets to build up α-ZrP/PAH/K$_4$Nb$_6$O$_{17}$/PAH heterostructures (Figure 3); the figure inset accentuates the dramatic thickness changes associated with the addition of specific individual layers. Importantly, the LBL technique is self-regulating because each immersion step deposits only one layer of polyanion or polycation.

An important benefit of using lamellar colloids to build up multilayer structures, instead of organic polyelectrolytes, is that sequentially grown layers do not necessarily interpenetrate. This feature is important if one wishes to use the ordered sequence of layers to avoid back electron transfer in photochemical electron-transfer cascades. The LBL assembly of sheets gives a "lasagne" structure, although in some cases (for example, with smectite clay sheets), there appears to be some mixing of components in sequential deposition steps.[37] We were able to show using fluorescence

Figure 3. Ellipsometric data for α-ZrP/PAH/K$_2$Nb$_6$O$_{17}$$^{2-}$/PAH LBL films. The inset shows the first derivative of the thickness for each adsorption step. Small and large peaks in the inset correspond to α-ZrP and K$_2$Nb$_6$O$_{17}$$^{2-}$ adsorption steps, respectively; the points between are PAH adsorption (from ref 24).

resonant energy-transfer techniques that α-ZrP layers do not interpenetrate significantly in LBL assemblies.[38] In this study, fluorescent probes were used as a spectroscopic ruler by measuring the efficiency of Förster energy transfer between successive layers. Polycationic PAH derivatized with either fluorescein (Fl) on rhodamine B (RhB), giving Fl−PAH and RhB−PAH polymers that contained approximately one dye molecule for every 20 and 50 monomeric units, respectively. LBL assemblies obtained by sequentially adsorbing α-ZrP and the fluorophore polycations onto 4-(aminobutyl)dimethylmethoxysilane/glass or 2-mercaptoethylamine/Au gave 22-Å-thick bilayers. The efficiency of Förster energy transfer, χ, can be used as a quantitative probe of intermolecular distances, r, because of the following relationship:[39]

$$\chi \approx \frac{R_0{}^6}{R_0{}^6 + r^6} \qquad (2)$$

At the Förster distance, R_0, the efficiency of the transfer is 0.5; for Fl and RhB, this distance has been determined to be 40 Å.[40] Experimentally, the efficiencies for the LBL assemblies were calculated by using either donor emission quenching or enhancement of the acceptor emission and values of χ from either method were typically within 2−5%.[39] Monte Carlo simulations were also performed to provide theoretical energy-transfer efficiencies using experimentally determined film thicknesses and densities of donors and acceptors. The experimental and simulated data correlated very well for a range of different layer sequences, providing compelling evidence that each adsorption step
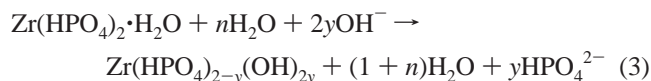
(25) Troup, J. M.; Clearfield, A. *Inorg. Chem.* **1977**, *16*, 3311.
(26) Decher, G.; Hong, J.-D. *Makromol. Chem., Macromol. Symp.* **1991**, *46*, 321.
(27) Decher, G.; Hong, J.-D.; Schmitt, J. *Thin Solid Films* **1992**, *210/211*, 504.
(28) Decher, G.; Schmitt, J. *Prog. Colloid Polym. Sci.* **1992**, *89*, 160.
(29) Decher, G. *Nachr. Chem., Tech. Lab.* **1993**, *41*, 793.
(30) Lvov, Y.; Decher, G.; Mohwald, H. *Langmuir* **1993**, *9*, 481.
(31) Lvov, Y.; Decher, G.; Sukhorukov, G. *Macromolecules* **1993**, *26*, 5396.
(32) Lvov, Y.; Hass, H.; Decher, G.; Mohwald, H.; Kalachev, A. *J. Phys. Chem.* **1993**, *97*, 12835.
(33) Lvov, Y.; Essler, F.; Decher, G. *J. Phys. Chem.* **1993**, *97*, 13773.
(34) Schmitt, J.; Grunewald, T.; Kjaer, K.; Pershan, P.; Decher, G.; Losche, M. *Macromolecules* **1993**, *26*, 7058.
(35) Johannson, G.; Lundgren, G.; Sillen, L. G.; Soderquist, R. *Acta Chem. Scand.* **1960**, 769.
(36) Takano, T.; Kallai, O. B.; Swanson, R.; Dickerson, R. E. *J. Biol. Chem.* **1973**, *248*, 5244.

(37) (a) Kleinfeld, E. R.; Ferguson, G. S. *Chem. Mater.* **1995**, *7*, 2329. (b) Kotov, N. A.; Dekany, I.; Fendler, J. H. *Adv. Mater.* **1996**, *8*, 637.
(38) Kaschak, D. M.; Mallouk, T. E. *J. Am. Chem. Soc.* **1996**, *118*, 4222.
(39) Lakowicz, J. R. *Principles of Fluorescence Spectroscopy*, 2nd ed.; Kluwer Academic/Plenum Publishers: New York, 1999.
(40) Wieb Van der Meer, B.; Coker, G.; Simon Chen, S.-Y. *Resonance Energy Transfer Theory and Data*; VCH: New York, 1994.

produces a monolayer and that successive organic layers have minimal interpenetration and are well-separated by the anionic sheets.

LBL assemblies were also prepared that incorporated *both* ionic and covalent interlayer connections.[41] In this "mix and match" strategy, α-ZrP sheets, deposited onto Au or Si substrates that were primed with thiol- or trialkoxysilyl-terminated phosphonic acids, were first charge-compensated by zirconium tetrameric hydroxycations, $[Zr_4(OH)_8(H_2O)_{16}]^{8+}$ (abbreviated as Zr_4^{8+}). A bis(phosphonic acid), C_nBPA, was then introduced, followed by sequential treatment with Zr_4^{8+} and α-ZrP sheets, giving the sequence α-ZrP/Zr_4^{8+}/C_nBPA/Zr_4^{8+}/α-ZrP. Such assemblies were constructed for $n = 4$, 8, 10, 12, 14, and 16. The thickness of the repeat sequence for $n = 16$ was determined to be 39 Å by ellipsometry and 41 Å by X-ray diffraction (Bragg peak at $2\theta = 2.1°$). Importantly, reflectance Fourier transform infrared spectroscopy showed that the intensity of both the asymmetric and symmetric CH_2 stretches were linear with the number of C_{16}-BPA layers, confirming the stepwise growth of the films. In the "mix and match" strategy, one can also switch from a covalent motif to an ionic one, as demonstrated by using intermittent α-ZrP/PAH bilayers.

Intercalation and exfoliation of α-ZrP sheets has been shown to compete with base hydrolysis/corrosion, as depicted by the following reaction:[42]

$$Zr(HPO_4)_2 \cdot H_2O + nH_2O + 2yOH^- \rightarrow$$
$$Zr(HPO_4)_{2-y}(OH)_{2y} + (1+n)H_2O + yHPO_4^{2-} \quad (3)$$

To minimize the corrosion process, α-ZrP sheets should be exfoliated at 0 °C, where the rate of hydrolysis is slow. A closer look at the base hydrolysis of α-ZrP sheets showed that the process occurs from the edges inward.[42] Atomic force microscopy revealed the presence of 1−10-nm-high "bumps" around the edges after heating of the sheets for 1 h in TBA^+OH^- at 75 °C. Further heating resulted in fewer sheets with a concomitant increase in the number of smaller particles. From transmission electron microscopy (TEM) images, the edges of the sheets displayed increased contrast following base hydrolysis, consistent with an increase in the electron density owing to the formation of hydrous zirconium oxide (relatively high electron density) and loss of phosphate groups (relatively low electron density). Indeed, inductively coupled plasma-atomic emission spectrometric analysis of solutions following restacking of the sheets by acidification with HCl indicated the presence of orthophosphate and negligible amounts of Zr, consistent with the loss of phosphate by hydrolysis.

Interestingly, it was found that the hydrolysis reaction was prevented by exfoliating the sheets in the presence of excess phosphate, suggesting that a dynamic equilibrium exists at the edges between phosphate and hydroxide anions.[42] The reversibility of the hydrolysis reaction was exploited by

selectively functionalizing the edges of the sheets with organophosphonates. Specifically, the sheets were exfoliated with TBA^+OH^- in the presence of vinylphosphonic acid to displace phosphate groups at the edge.[42] The olefinic groups of vinylphosphonic acid were then reacted with OsO_4, gradually resulting in the formation of 2−20-nm colloids of, presumably, OsO_2. TEM images showed that the sheet edges were almost entirely decorated with OsO_2 nanoparticles. Control experiments in which phosphate edge groups were displaced by ethylphosphonic acid showed that the OsO_2 nanoparticles[43] were randomly associated with the sheets and that hydrolysis of the edges was significantly diminished.

Other materials for preparing inorganic sheets by exfoliation for use in LBL assemblies have been identified. These include Dion−Jacobsen layered perovskites (A[$A_{n-1}'B_nO_{3n+1}$], where A = alkali, A′ = alkaline earth or rare earth, and B = transition metal),[44,45] Ruddlesden−Popper layered perovskites ($A_2[A_{n-1}'B_nO_{3n+1}]$),[46] and layered tritutile phases ($HMWO_6$, M = Nb, Ta).[47] Interestingly, in some cases, exfoliation of acid-exchanged Ruddlesden−Popper layered perovskites forms both nanoscale sheets and cylindrical scrolls.[46] Scrolling of sheets upon exfoliation has been extensively studied with acid-exchanged $K_4Nb_6O_{17}$.[48] Recent experiments by Ma and co-workers have shown that the scrolling of lamellar colloids is a general phenomenon and that many different types of materials can be fabricated as tubular and conical nanostructures.[49]

Electron/Energy-Transfer Assemblies. As noted above, there is considerable interest in creating artificial photosynthetic devices that can efficiently harness solar energy, *vectorially* separate electrons and holes, and produce useful fuels with these redox equivalents.[50] Vectorial movement of holes and electrons is a key first step because it minimizes undesirable charge recombination and promotes successful conversion of the stored potential energy into chemical energy.

Artificial photosynthesis is often studied using molecular-based synthetic systems containing several redox-active components with the ultimate goal of developing efficient photoconversion systems or devices.[1] In triad systems, for example, charge separation is typically afforded by excited-state electron transfer from a visible-light-absorbing spacer (S) to a covalently attached acceptor component (A), followed by thermal electron transfer from a donor component (D) to the oxidized spacer:[51,52]

$$D-S-A \xrightarrow{h\nu} D-S^*-A \rightarrow D-S^+-A^- \rightarrow D^+-S-A^- \quad (4)$$

(41) Fang, M. M.; Kaschak, D. M.; Sutorik, A. C.; Mallouk, T. E. *J. Am. Chem. Soc.* **1997**, *119*, 12184.

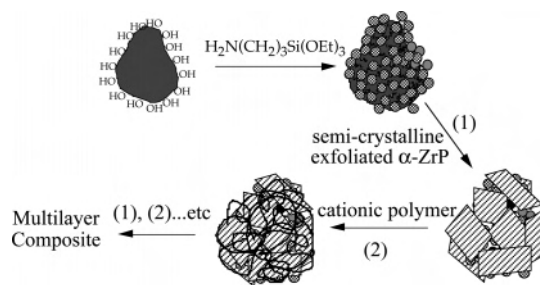(42) Kaschak, D. M.; Johnson, S. A.; Hooks, D. E.; Kim, H. N.; Ward, M. D.; Mallouk, T. E. *J. Am. Chem. Soc.* **1998**, *120*, 10887.

(43) Hayat, M. A. *Fixation for Electron Microscopy*; Academic Press: New York, 1981.

(44) Fang, M. M.; Kim, C. H.; Saupe, G. B.; Kim, H. N.; Waraksa, C. C.; Miwa, T.; Fujishima, A.; Mallouk, T. E. *Chem. Mater.* **1999**, *11*, 1526.

(45) Schaak, R. E.; Mallouk, T. E. *Chem. Mater.* **2000**, *12*, 2513.

(46) Schaak, R. E.; Mallouk, T. E. *Chem. Mater.* **2000**, *12*, 3427.

(47) Schaak, R. E.; Mallouk, T. E. *Chem. Commun.* **2002**, 706.

(48) Saupe, G. B.; Waraksa, C. C.; Kim, H. N.; Han, Y. J.; Kaschak, D. M.; Skinner, D. M.; Mallouk, T. E. *Chem. Mater.* **2000**, *12*, 1556.

(49) Ma, R.; Bando, Y.; Sasaki, T. *J. Phys. Chem. B* **2004**, *108*, 2115−2119.

This motif has been expanded with supermolecules containing up to five different redox-active subunits, all of which participate in the multistep charge-separation reaction.[53]

Quantum yields for charge separation critically depend on the branching ratio between forward and back-electron-transfer rates at each successive step within the multicomponent system and can only approach unity if the forward pathway is the kinetically dominant one.[1] By tuning the electronic coupling and thermodynamic driving of each successive electron-transfer step, near-unity quantum yields and extremely long charge-separation lifetimes have been achieved.[54,55]

While these multicomponent systems are quite useful for modeling aspects of natural photosynthesis, their synthesis becomes increasingly demanding as more chromophoric or redox-active units are added.[56] In addition, these systems are typically studied in fluid solution or frozen glasses where the charge-separated state ultimately decays back to the ground state. To utilize the redox equivalents of the charge-separated state, the molecules should be organized in space at a level of complexity and control required for high conversion efficiencies.[56] Ideally, organization of the photoredox/redox-active molecules would be achieved through an assembly process, avoiding the need for covalent linkages between all of the components.
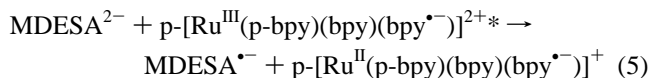
LBL assembly of photosystems using inorganic sheets was demonstrated by Keller et al., who grew concentric "onion" structures on high surface area silica (average diameter = 50 nm).[56−58] Utilization of high surface area particles provides good signal-to-noise ratios in flash photolysis experiments, allowing one to observe the charge-separated products and determine quantum yields and kinetics (vide infra). Fumed silica particles were first derivatized with (3-aminopropyl)trimethoxysilane, washed, dried, and then exposed to a suspension of exfoliated α-ZrP sheets ($\sim$15 $\times$ 15 $\times$ 0.8 nm). Following centrifugation and washing, methylviologen-functionalized polystyrene (p-MV^{2+}) was deposited from aqueous solution, followed sequentially by another layer of α-ZrP sheets and a polystyrene layer functionalized with a ruthenium(II) poly(pyridyl) photosensitizer (p-[Ru^{III}(p-bpy)(bpy)$_2$)]$^{2+}$, abbreviated as p-Ru^{2+}, where bpy is 2,2′-bipyridine and p-bpy is the 2,2′-bipyridine ligand directly attached to the polymeric backbone; Figures
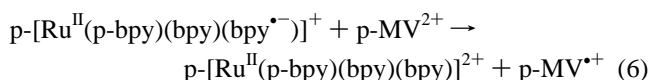

Figure 4. Schematic procedure for the preparation of the composite multilayers on high-surface-area silica.

4 and 5). On planar Si surfaces, deposition of the polycationic redox layers reproducibly gave thicknesses of $\sim$9 Å by ellipsometry, while the α-ZrP layers had thicknesses consistent with previous results.

Visible-light absorption by p-Ru^{2+} produces a metal-to-ligand charge-transfer (MLCT) excited state (formally p-[Ru^{III}(p-bpy)(bpy)(bpy$^{•−}$)]$^{2+}$) that is a potent reductant [$E(Ru^{3+/2+}*)$ $\sim$ −0.62 V vs NHE] capable of transferring an electron to p-MV^{2+} [$E(MV^{2+/+})$ = −0.45 V vs NHE]. Surprisingly, when p-MV^{2+} was deposited prior to p-Ru^{2+} (i.e., p-Ru^{2+}/α-ZrP/p-MV^{2+}/α-ZrP/SiO$_2$), photoexcitation with 532-nm pulsed-laser light did not produce $MV^{•+}$. In addition, the excited-state lifetime (600 ns) was similar to that observed for p-Ru^{2+}/α-ZrP/SiO$_2$, suggesting minimal quenching of p-$Ru^{2+}*$ by p-MV^{2+}. In contrast, when the reversible electron donor, methoxy-N,N-bis(ethylsulfonate) (MDESA$^{2−}$), was added to the solution containing p-Ru^{2+}/α-ZrP/p-MV^{2+}/α-ZrP/SiO$_2$, a p-$MV^{•+}$/MDESA$^−$ charge-separated state was observed with a quantum yield of $\sim$30%. MDESA$^{2−}$ reduces the metal center of p-$Ru^{2+}*$, forming a Ru$^+$ species in which one of the bipyridine ligands remains reduced:
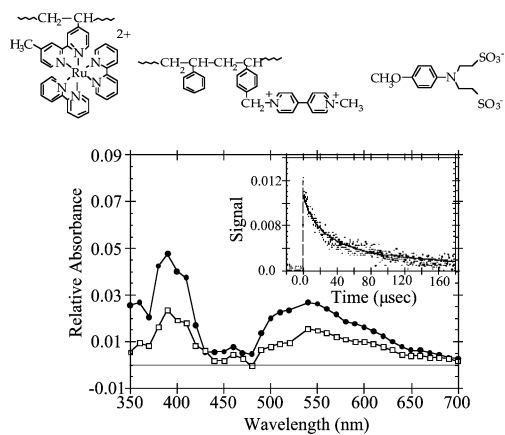
$$\text{MDESA}^{2-} + \text{p-[Ru}^{III}(\text{p-bpy})(\text{bpy})(\text{bpy}^{•-})]^{2+}* \rightarrow$$
$$\text{MDESA}^{•-} + \text{p-[Ru}^{II}(\text{p-bpy})(\text{bpy})(\text{bpy}^{•-})]^{+} \quad (5)$$

Experiments performed without p-MV^{2+} indicated that excited-state reduction of p-$Ru^{2+}*$ by MDESA$^{2−}$ occurs with a yield of $\sim$50% and involves both dynamic and static components, the latter of which is made possible by ground-state adducts between oppositely charged donor and acceptor compounds. Importantly, the Ru$^+$ species is a more powerful reductant than Ru$^{2+}*$ by $\sim$0.4 V, providing the extra driving force needed to create an interlayer charge-separated state:

$$\text{p-[Ru}^{II}(\text{p-bpy})(\text{bpy})(\text{bpy}^{•-})]^{+} + \text{p-MV}^{2+} \rightarrow$$
$$\text{p-[Ru}^{II}(\text{p-bpy})(\text{bpy})(\text{bpy})]^{2+} + \text{p-MV}^{•+} \quad (6)$$

Charge recombination followed second-order kinetics and occurred on the microsecond time scale ($k_{obs} = 1 \times 10^9$ M^{-1} s^{-1}), consistent with MDESA$^{•−}$ escaping the p-Ru^{2+} layer (escape yield $\sim$ 60%). Hence, charge recombination requires diffusion of MDESA$^{•−}$ through *both* p-Ru^{2+} and anionic α-ZrP layers. Interestingly, when the order of polymer deposition was reversed, i.e., p-MV^{2+}/α-ZrP/p-Ru^{2+}/α-ZrP/SiO$_2$, p-$Ru^{2+}*$ was no longer quenched by MDESA$^{2−}$ and charge separation was no longer observed with or without the electron donor. Apparently, diffusion of MDESA$^{2−}$ to
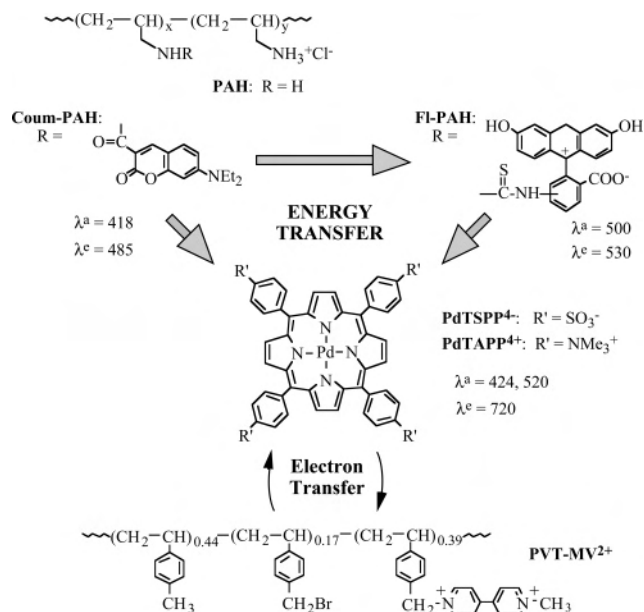
(50) Wasielewski, M. R. *Chem. Rev.* **1992**, *92*, 435.
(51) Kodis, G.; Liddell, P. A.; de la Garza, L.; Clausen, C.; Lindsey, J. S.; Moore, A. L.; Moore, T. A.; Gust, D. *J. Phys. Chem. A* **2002**, *106*, 2036.
(52) Miller, S. E.; Lukas, A. S.; Marsh, E.; Bushard, P.; Wasielewski, M. R. *J. Am. Chem. Soc.* **2000**, *122*, 7802.
(53) Gust, D.; Moore, T. A.; Moore, A. L. *Acc. Chem. Res.* **1993**, *26*, 198.
(54) Gust, D.; Moore, T. A.; Moore, A. L.; Lee, S.-J.; Bittersman, E.; Juttrull, D. K.; Rehms, A. A.; DeGraziano, J. M.; Ma, X. C.; Gao, F.; Belford, R. E.; Trier, T. T. *Science* **1990**, *248*, 199.
(55) Gust, D.; Moore, T. A.; Moore, A. L.; Macpherson, A. N.; Lopez, A.; DeGraziano, J. M.; Gouni, I.; Bittersman, E.; Seely, G. R.; Gao, F.; Nieman, R. A.; Ma, X. C.; Demanche, L.; Hung, S.-C.; Luttrell, D. K.; Lee, S.-J.; Kerrigan, P. K. *J. Am. Chem. Soc.* **1993**, *115*, 11141.
(56) Kaschak, D. M.; Lean, J. T.; Waraksa, C. C.; Saupe, G. B.; Usami, H.; Mallouk, T. E. *J. Am. Chem. Soc.* **1999**, *121*, 3435.
(57) Keller, S. W.; Johnson, S. A.; Brigham, E. S.; Yonemoto, E. H.; Mallouk, T. E. *J. Am. Chem. Soc.* **1995**, *117*, 12879.
(58) Kaschak, D. M.; Johnson, S. A.; Waraksa, C. C.; Pogue, J.; Mallouk, T. E. *Coord. Chem. Rev.* **1999**, *186*, 403.

Figure 5. Top: Structures of p-Ru^{2+}, p-MV^{2+}, and MDESA^{2-}. Bottom: Transient diffuse-reflectance spectra for a p-Ru^{2+}/p-MV^{2+}/SiO$_2$ composite with 3.5 mM MDESA^{2-} in solution at 10 μs (filled circles) and 40 μs (open squares) following 532 nm, 7-ns laser excitation. The inset shows the transient signal of the viologen cation radical recorded at 400 nm and a second-order fit to the data (solid line).

the buried p-Ru^{2+} layer is severely impeded in this composite such that MDESA^{2-}/Ru^{2+} ground-state adducts no longer form and diffusional quenching between MDESA^{2-} and p-Ru^{2+}* no longer occurs. In addition, when the α-ZrP sheets were replaced with organic poly(styrenesulfonate) (PSS), reaction (5) was no longer observed presumably because p-Ru^{2+} is intertwined with anionic PSS, preventing the approach of MDESA^{2-}. In the absence of the silica support, i.e., when p-Ru^{2+}, p-MV^{2+}, and MDESA^{2-} were dissolved together in solution, reaction (5) was observed while reaction (6) was not, presumably because of repulsion between the polycationic redox polymers.

The successful demonstration of photoinduced charge separation in this D−S−A "onion" system suggested the possibility of making a more complex artificial photosynthetic system by LBL techniques. In this multilayer thin film system, light absorption was coupled to electron transfer/ charge separation by a series of energy transfers through an antenna system containing three dye molecules (Figure 6).[56] The dyes that were chosen, coumarin, Fl, and a tetrasubstituted palladium(II) tetraphenylporphyrin (PdTPP), have large molar extinction coefficients and absorb visible light at progressively longer wavelengths. In order for Förster (i.e., singlet−singlet) energy transfer to be efficient, good spectral overlap must exist between the donor emission spectra and the acceptor absorbance spectra.[39] Accordingly, the coumarin dye absorbs light in the blue region of the visible spectrum ($\lambda_{abs,max}$ = 412 nm; λ_{em} = 485 nm) and can donate its excited-state energy to the Fl dye ($\lambda_{abs,max}$ = 500 nm; λ_{em} = 530), which, in turn, can transfer its excited-state energy to PdTPP ($\lambda_{abs,max}$ = 520 nm; λ_{em} = 720 nm). It is also possible for the coumarin dye to transfer energy directly to the porphyrin dye because the coumarin emission and porphyrin Q-band absorbance slightly overlap. Importantly, porphyrin excited states are formed either by direct excitation or indirectly by excitation of the coumarin or Fl dyes. Furthermore, the presence of a Pd atom in the porphyrin fluorophore ensures nearly quantitative intersystem crossing to a long-lived triplet
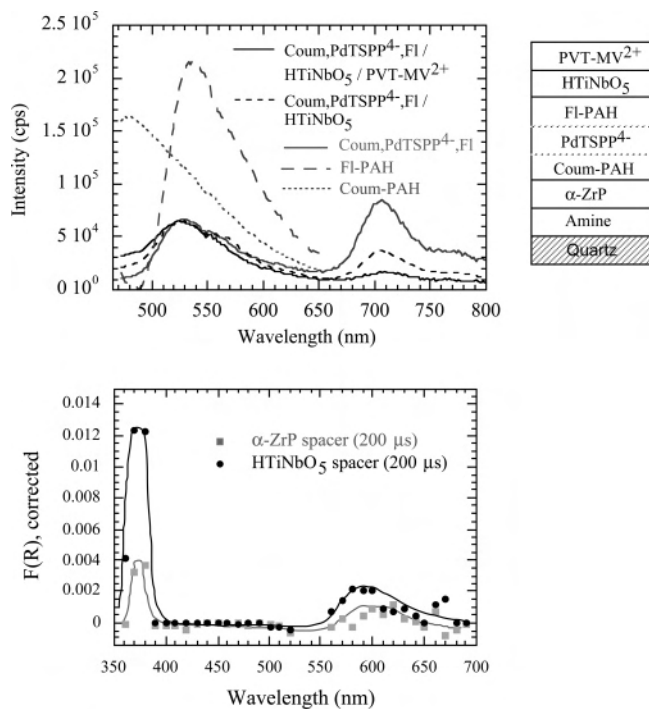

Figure 6. Molecular structures and energy- and electron-transfer pathways (indicated by arrows) for the energy "antenna" polymers, Coum-PAH and Fl-PAH; the photosensitizers, PdTAPP^{4+} and PdTSPP^{4-}; and the electron-acceptor polymer, PVT-MV^{2+}.

excited state, allowing ample time for interlayer electron transfer to occur.[56]

Two kinds of multilayer thin film assemblies were prepared through alternate anion/cation adsorption steps. For *interlayer* energy transfer, coumarin-functionalized PAH (Coum-PAH), Fl-functionalized PAH (Fl-PAH), and palladium(II) tetrakis(4-N,N,N-trimethylanilinium)porphyrin (i.e., PdTPP^{4+}) were deposited sequentially using anionic α-ZrP layers as spacers.[56] For *intralayer* energy transfer, all three polycationic dyes were adsorbed simultaneously onto anionic α-ZrP. Absorption and emission spectra of both multilayer assemblies were obtained and compared with that for individual dye layers. The emission spectra (excitation with 450 nm) showed almost complete quenching for the coumarin dye, significant quenching of the Fl dye, and enhanced emission from the porphyrin. On the basis of the emission data, the energy-transfer efficiency of the *interlayer* assembly was calculated to be 0.65 while that for the *intralayer* assembly was 0.82. The lower efficiency of the *interlayer* assembly was attributed to the Förster distances of the various donor−acceptor combinations being close to the α-ZrP/dye-PAH bilayer thickness (∼22 Å). In contrast, the average donor−acceptor distances in the *intralayer* assembly were significantly smaller, allowing for relatively facile energy transfer.[56]

Because the intralayer assembly gave superior results, it was coupled to an electron-acceptor layer, methylviologen-functionalized poly(vinyltoluene) (PVT-MV^{2+}; Figure 7). To provide a larger driving force for electron transfer from the porphyrin excited state to MV^{2+}, PdTPP^{4+} was replaced with a tetraanionic porphyrin (PdTPP^{4-}), which is a more powerful triplet excited-state reductant by ∼0.3 V.[56] Efficient quenching of the porphyrin phosphorescence was observed upon the addition of PVT-MV^{2+} to the system, the degree of which depended on the anionic "glue" used for its fastening. Using

Figure 7. Top: Emission (λ_{ex} = 450 nm) spectra of an energy/electron-transfer assembly with a HTiNbO$_5$ spacer separating the porphyrin and viologen layers. Dotted lines in the idealized picture at the right indicate a mixed Coum-PAH, PdTSPP^{4-}, and Fl-PAH polyelectrolyte layer. Reference spectra from individual chromophore layers (Coum-PAH, PdTSPP^{4-}, and Fl-PAH) and from the triad without PVT-MV^{2+} are also shown. Bottom: Transient diffuse-reflectance spectra taken 200 μs after 532 nm excitation, for silica/amine/α-ZrP/PVT-MV^{2+}/α-ZrP/PAH/PdTSPP^{4-} (lower gray spectrum), and silica/amine/α-ZrP/PVT-MV^{2+}/HTiNbO$_5$/PAH/PdTSPP^{4-} (upper black spectrum) samples.
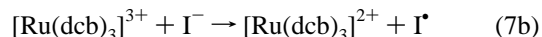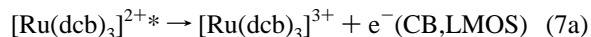
HTiNbO$_5$ sheets, the phosphorescence was quenched by 76% while that for α-ZrP was 58%. This corresponds to combined energy/electron-transfer quantum yields of 0.61 and 0.47, respectively. Importantly, spectra from diffuse-reflectance flash photolysis experiments for similar systems constructed on high surface area silica showed that MV$^{\bullet+}$ is present on the microsecond time scale and that it is produced in greater yield when the HTiNbO$_5$ spacer is used. These results suggested that semiconducting HTiNbO$_5$ sheets mediate the electron transfer between ^{3}PdTPP^{4-}* and MV^{2+}, while α-ZrP, an insulator, does not. Indeed, when HTiNbO$_5$ is layered on the top of the intralayer assembly in the absence of PVT-MV^{2+}, significant quenching of ^{3}PdTPP^{4-}* phosphorescence is observed, suggesting that electron transfer between ^{3}PdTPP^{4-}* and HTiNbO$_5$ is occurring.[56]

Photocatalytic Generation of Hydrogen and Oxygen

Nonsacrificial Hydrogen-Evolving Photosystems. As noted above, many artificial photosynthetic systems have been constructed with the purpose of transiently separating charge, or generating products from sacrificial reagents. Structural control is really most needed when nonsacrificial reagents are used because of the possibility of recombination reactions. Catalysts for generating chemical products should be spatially compartmentalized and connected by an electron relay system that disfavors charge recombination. The recombination reaction is necessarily thermodynamically

downhill and favorable because free energy is stored in the charge-separated state. Compartmentalization of redox reactions is conveniently achieved in photoelectrochemical cells by carrying out oxidation and reduction reactions at spatially well-separated electrodes. However, in photochemical systems, oxidation and reduction products are typically made at the same particle. Therefore, preventing their recombination requires sieving at the molecular level.

In the first example of such a nonsacrificial artificial photosynthetic system, LMOS sheets of K$_{4-x}$H$_x$Nb$_6$O$_{17}$·nH$_2$O ($x \sim 2.5$) were sensitized with [Ru(dcb)$_3$]$^{2+}$ (where dcb is 4,4′-dicarboxylic acid−2,2′-bipyridine).[59,60] The sensitization strategy in this case is similar to that used successfully in dye-sensitized photoelectrochemical cells[61] and in colloidal semiconductor systems.[62] Visible-light excitation produces the MLCT excited state [Ru(dcb)$_3$]$^{2+*}$, which is capable of injecting an electron into the conduction band (CB) of the semiconducting sheets. Spectra obtained by transient diffuse-reflectance/laser flash photolysis experiments (532 nm pulsed-laser excitation) displayed a bleach from 400 to 600 nm, consistent with the formation of a Ru^{3+}/e$^-$(CB,LMOS) charge-separated state, which recombines within 100 μs and follows biphasic kinetics. In the presence of the electron donor, KI, [Ru(dcb)$_3$]$^{3+}$ is no longer observed by flash photolysis; instead, a positive transient at 380 nm is observed and attributed to the formation of I$_2^{\bullet-}$ according to the following reaction sequence:

$$[\text{Ru(dcb)}_3]^{2+*} \rightarrow [\text{Ru(dcb)}_3]^{3+} + \text{e}^-(\text{CB,LMOS}) \quad (7a)$$

$$[\text{Ru(dcb)}_3]^{3+} + \text{I}^- \rightarrow [\text{Ru(dcb)}_3]^{2+} + \text{I}^\bullet \quad (7b)$$

$$\text{I}^\bullet + \text{I}^- \rightarrow \text{I}_2^{\bullet-} \quad (7c)$$

$$2\text{I}_2^{\bullet-} \rightarrow \text{I}_3^- + \text{I}^- \quad (7d)$$

Hence, the charge-separated state on the microsecond time scale consists of I$_2^{\bullet-}$/e$^-$(CB,LMOS), formed with a quantum yield of $\sim$10−15%. On a seconds-to-minutes time scale, only triiodide is observed, showing that I$_2^{\bullet-}$ has disappeared either by disproportionation (eq 7d) or by recombination with injected CB electrons.[63]

To utilize the reducing equivalents of the charge-separated state for hydrogen evolution, the LMOS sheets were internally platinized. This process, which was first reported by Domen and co-workers, involves ion exchange of Pt(NH$_3$)$_4^{2+}$ ions into the interlayer galleries, followed by hydrogen reduction at 200−600 °C.[64] Aqua regia treatment is then used to remove Pt from external sites. Because the solid is a cation exchanger, the resulting interlayer Pt clusters are inaccessible

(59) Kim, Y. I.; Salim, S.; Huq, M. J.; Mallouk, T. E. *J. Am. Chem. Soc.* **1991**, *113*, 9561.
(60) Kim, Y. I.; Atherton, S. J.; Brigham, E. S.; Mallouk, T. E. *J. Phys. Chem.* **1993**, *97*, 11802.
(61) Grätzel, M. *Nature* **2001**, *414*, 338.
(62) Kamat, P. V. *Chem. Rev.* **1993**, *93*, 267.
(63) Saupe, G. B.; Mallouk, T. E.; Kim, W.; Schmehl, R. H. *J. Phys. Chem. B* **1997**, *101*, 2508.
(64) Domen, K.; Yoshimura, J.; Sekine, T.; Tanaka, A.; Onishi, T. *Catal. Lett.* **1990**, *4*, 339.

to anions. For example, $[Fe(CN)_6]^{3-}$ is not reduced by molecular hydrogen in the presence of platinized sheets prepared by this method. This suggests that anionic species, such as I_3^-, are incapable of intralayer diffusion and recombination with molecular hydrogen.

Hydrogen evolution was tested by photolyzing the above system using a Hg−Xe lamp. Upon light excitation, hydrogen and triiodide are formed in equimolar amounts. Importantly, hydrogen is formed in trace amounts in the absence of iodide and is not formed in the absence of $[Ru(dcb)_3]^{2+}$. The initial quantum yield was determined to be ∼0.3%; because this is a factor of 40 lower than that determined by flash photolysis, the major recombination pathway involves the reduction of I_3^- or $I_2^{•-}$ by injected electrons in the semiconductor. Over time, the hydrogen evolution plateaus as the concentration of triiodide increases. When a fresh iodide solution is introduced and the photolysis reaction is resumed, the initial hydrogen evolution rate is restored, supporting the claim that CB electrons also recombine with triiodide. Importantly, when photolysis is stopped, the triiodide and hydrogen levels of the system do not change, indicating that back reaction between photoproducts does not occur appreciably, presumably a result of their physical separation.

In later studies, several LMOSs were studied as components in the above system: acid-exchanged titanates (Na_3-Ti_3O_7 and $K_2Ti_4O_9$), niobates (KNb_3O_8 and $K_4Nb_6O_{17}$), and titanoniobates ($KTiNbO_5$ and $CsTi_2NbO_7$).[60] Following selective internal platinization, the LMOSs were fully acid-exchanged; suspensions prior to acid exchange gave pH = 9−10, while those afterward gave pH = 3−4. Photochemical (>400 nm) hydrogen evolution was measured by gas chromatography for sensitized, internally platinized LMOSs in the presence of iodide. Only the niobates and titanoniobates were found to produce stoichiometric amounts of hydrogen and triiodide, with $K_4Nb_6O_{17}$ giving the highest initial quantum yield. In contrast, only trace amounts of hydrogen were detected for the two titanates under similar conditions. These results were attributed to the titanates having relatively positive CB-edge energies compared to the niobates and titanoniobates. Theoretical predictions of the LMOS's band-edge energies were made using concepts of electronegativity. The CB-edge energy at the point of zero charge of a semiconductor, E_{cs}^0, can be expressed by[65]

$$E_{cs}{}^0 = E^e - X + (1/2)E_g \qquad (8)$$

where E^e is the energy of free electrons on the hydrogen scale (∼4.5 eV), X is the electronegativity of the semiconductor (calculated as the geometric mean of the electronegativities of its constituent atoms[66]), and E_g is the bandgap energy of the semiconductor. Importantly, predicted values attained by this method have been shown to reasonably agree with experimentally determined flat band potentials.[67] Using the above equation, the estimated CB-edge

energies for alkali LMOSs (∼ −0.6 to −0.9 V vs NHE) tended to more negative than that of anatase TiO_2 (−0.3 V) while those of acid-exchanged LMOSs tended to be more positive (∼0 V). Experimental support of this trend was obtained from pH-dependent photoluminescence quenching experiments of $[Ru(dcb)_3]^{2+}$ on TiO_2 and on LMOSs. On TiO_2, significant quenching was only observed when the pH was adjusted below 6, while that for the LMOSs began at pH = 4.5. This result is in qualitative agreement with the LMOSs having more negative CB-edge energies than TiO_2.

Interestingly, when the acid-exchanged niobates and titanoniobates were suspended in alkali iodide solutions, the pH of the suspension dropped from 3−4 to 1−2 because of the exchange of protons for alkali cations. This behavior was *not* observed for the titanates. X-ray diffraction studies corroborated this, showing the presence of an additional interlayer spacing for the niobates and titanoniobates that have undergone alkali iodide treatment. In contrast, the titanates showed no changes in their diffraction patterns. Hence, the niobates and titanoniobates were partially proton-exchanged under the photolysis conditions used while the titanates remained fully acidified. As a result, the CB-edge energies of the niobates and titanoniobates should be more negative than those of the titanates. Furthermore, the slightly more acidic conditions used for the titanoniobates and niobates pushes the water/hydrogen reduction potential more positive, favoring hydrogen evolution. It was concluded that the titanates did not evolve hydrogen effectively because injected electrons cannot reduce protons and thus fall victim to recombination. Similar explanations were used in followup studies to explain the superior photochemical hydrogen evolution observed for zeolite L impregnated with Nb_2O_5 and Pt in the presence of the nonsacrificial electron donor, $MDESA^{2-}$, as compared to that impregnated with TiO_2 and Pt.[68]

The hydrogen evolution rate was also shown to critically depend on the LMOS interlayer spacing.[60] The spacing was varied by changing the iodide's countercation, decreasing in the order Na > Li > Cs > K > H.[69] The evolution rate increased in the same order, suggesting that a competition exists between charge recombination and electron tunneling between layers. In a layered LMOS system, the photosensitizer is adsorbed only on the external surface; thus, injected electrons reach Pt deposits faster when the interlayer spacing is small.

On strategy for potentially reducing the rate of charge recombination involves blocking the access of $I_2^{•-}$ and/or I_3^- to the LMOS surface. This was initially attempted by adsorbing alkyl phosphonates to $[Ru(dcb)_3]^{2+}$-sensitized LMOS surfaces. Unfortunately, this resulted in significant sensitizer desorption under aqueous conditions. To circumvent this problem, a subsequent study employed a sensitizer that attaches itself to the LMOS surface through an aryl

(65) Morrison, S. R. *Electrochemistry at Semiconductor and Oxidized Metal Electrodes*; Plenum Press: New York, 1980.
(66) Sanderson, R. T. *Chemical Periodicity*; Reinhold: New York, 1960.
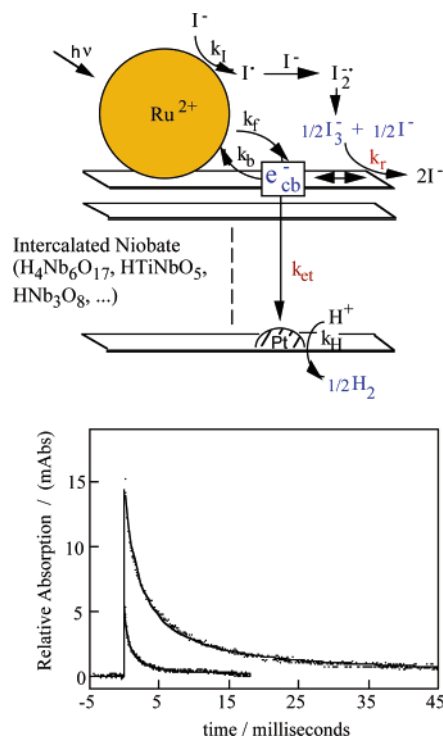(67) Butler, M. A.; Ginley, D. S. *J. Electrochem. Soc.* **1978**, *125*, 228.
(68) Kim, Y. I.; Keller, S. W.; Krueger, J. S.; Yonemoto, E. H.; Saupe, G. B.; Mallouk, T. E. *J. Phys. Chem. B* **1997**, *101*, 2491.
(69) Kinomura, N.; Kumada, N.; Muto, F. *J. Chem. Soc., Dalton Trans.* **1985**, 2349.
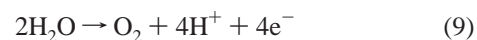
Figure 8. Top: Schematic drawing of an internally platinized, sensitized LMOS system showing kinetic pathways for photoinduced charge injection, charge recombination, and hydrogen evolution from an iodide solution. Bottom: Average of 20 transient diffuse-reflectance traces, acquired at 380 nm, for $K_{4-x}H_xNb_6O_{17}$ sensitized by (bpy)$_2$Ru(4-(2,2′-bipyrid-4-yl)phen-ylphosphonic acid and for a similar sample modified with PSS, showing the difference in time scales for the charge recombination reaction of e_{CB}^- and I_3^-. Second-order fits (solid lines) are superimposed on the data points.

phosphonate linkage.[63] Two polyanionic surface modifiers were examined, $[TiNbO_5]_n^{n-}$ and PSS. Because the sensitizer imparts a positive charge to the unmodified LMOS surface, it is possible to deposit an anionic layer on top. Treatment of a sensitized surface (1.43 μmol/g of LMOS) with excess aqueous PSS resulted in a surface coverage of 5.25 μmol of PSS/g of LMOS, indicating that the PSS layer overcompensates the charge of the sensitizer and provides a net negative charge to the surface. Both $[TiNbO_5]_n^{n-}$ and PSS were shown to increase the initial hydrogen evolution rate by a factor of 3 and 5, respectively (Figure 8). In the case of PSS, the initial rate corresponds to a quantum yield of 3%. The polyanionic layer presumably assists in excluding redox-active species such as $I_2^{\bullet-}$ and I_3^- from the surface, thus decreasing the rate of charge recombination between these species and the injected electrons within the LMOS structure. This idea is supported by transient diffuse-reflectance spectra obtained with and without PSS (Figure 8). The decays for charge recombination are well-described by a second-order kinetic model with rate constants of 3.17 ($\pm$0.03) $\times 10^7$ and 3.01 ($\pm$0.03) $\times 10^6$ M^{-1} s^{-1} for the unmodified and PSS-modified samples, respectively. While the actual values of these rate constants depend on an assumption about the path length of the analyzing light, the ratio of the rate constants (approximately 10) does not and is in semiquantitative agreement with the enhanced hydrogen evolution rate found in the presence of PSS.
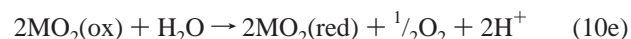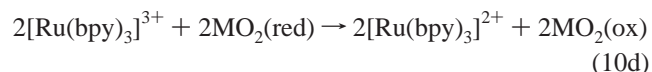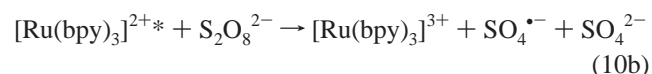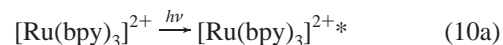
The time scale of charge recombination is several milliseconds in the PSS-modified system. It follows that, in order to replace iodide by water as the electron donor, one would need to couple this system to an oxygen-evolving catalyst that could turn over quite rapidly. Alternatively, it may be possible to modify the solid to increase the rate of electron transfer from the outer surface, which is where electrons are injected, to interlayer Pt clusters. The low quantum yield for hydrogen evolution indicates that the time scale of this process is long (tens to hundreds of milliseconds) in LMOS systems, where electronic coupling between sheets is relatively weak.

Water Oxidation Catalysis. One of the biggest obstacles to achieving efficient photochemical water splitting has been the inability to identify an effective, selective O$_2$-evolving system. Because the evolution of O$_2$ from H$_2$O requires four oxidizing equivalents [reaction (9)], this process is kinetically

$$2H_2O \rightarrow O_2 + 4H^+ + 4e^- \tag{9}$$

more demanding than hydrogen evolution. While there has been encouraging progress with transition-metal−oxo-bridged clusters as homogeneous oxygen evolution catalysts,[70−76] none have turnover rates faster than about 0.01 s^{-1}. The exception is the Mn$_3$CaO$_4$ cluster of photosystem II in natural photosynthesis, which has a turnover rate on the order of 10^3 s^{-1}.[77]

It has long been known that colloidal and bulk RuO$_2$ and IrO$_2$ are capable of heterogeneously catalyzing water oxidation in the presence of a [Ru(bpy)$_3$]$^{2+}$ photosensitizer and the sacrificial electron acceptor, S$_2$O$_8^{2-}$, via photocatalytic cycle (10).[78−82] The mechanism involves the following elementary steps:

$$[Ru(bpy)_3]^{2+} \xrightarrow{h\nu} [Ru(bpy)_3]^{2+*} \tag{10a}$$

$$[Ru(bpy)_3]^{2+*} + S_2O_8^{2-} \rightarrow [Ru(bpy)_3]^{3+} + SO_4^{\bullet-} + SO_4^{2-} \tag{10b}$$

$$[Ru(bpy)_3]^{2+} + SO_4^{\bullet-} \rightarrow [Ru(bpy)_3]^{3+} + SO_4^{2-} \tag{10c}$$

$$2[Ru(bpy)_3]^{3+} + 2MO_2(red) \rightarrow 2[Ru(bpy)_3]^{2+} + 2MO_2(ox) \tag{10d}$$

$$2MO_2(ox) + H_2O \rightarrow 2MO_2(red) + \tfrac{1}{2}O_2 + 2H^+ \tag{10e}$$

In the absence of any of the above components, no O$_2$ is observed. The initial quantum yields for O$_2$ evolution have been found to reach 40−60% under optimized conditions.[8] The [Ru(bpy)$_3$]$^{2+}$ photosensitizer, however, is irreversibly consumed during the photocatalytic cycle, and in phosphate-containing buffers, its turnover number does not exceed 80 even under the most optimized conditions.[8] Decomposition

(70) Naruta, Y.; Sasayama, M.; Sasaki, T. *Angew. Chem., Int. Ed.* **1994**, *33*, 1839.
(71) (a) Hammarstrom, L.; Sun, L.; Akermark, B.; Styring, S. *Catal. Today* **2000**, *58*, 57−69. (b) Sun, L.; Hammarstrom, L.; Akermark, B.; Styring, S. *Chem. Soc. Rev.* **2001**, *30*, 36−49.
(72) Khairutdinov, R. F.; Hurst, J. K. *Nature* **1999**, *402*, 509−511.

of the sensitizer is believed to involve nucleophilic attack by H_2O upon one or more of $[Ru(bpy)_3]^{3+}$'s bipyridine ligands.[83] Whereas both RuO_2 and IrO_2 can catalyze O_2 evolution, bulk and colloidal IrO_2 has been found to be more stable than RuO_2, which undergoes anodic corrosion.[80,81]

Colloidal IrO_2 is a particularly interesting colloidal catalyst because of its stability and the ease of analysis of the photocatalytic cycle (10) with simple UV−vis spectrophotometry.[84] Colloidal catalysts also typically have a surface charge that can be used to incorporate them into photosynthetic assemblies constructed from inorganic sheets and organic polyelectrolytes.[82] As a result, the photocatalytic potential of IrO_2 colloids has been further investigated in this laboratory beyond the previous studies by Harriman and co-workers.

In photoredox cycle (10), protons are released when O_2 is evolved, and this causes a decrease in the pH of the system. Harriman and co-workers have shown that the reduction potential of IrO_2 colloids shifts positively as the pH of the external solution is lowered.[85] At lower pH, the driving force for reaction (10d) decreases, leading to slower electron transfer between the photosensitizer and IrO_2(red). At higher pH, nucleophilic attack on the oxidized Ru(III) complex becomes more rapid. Hence, it is advantageous to control the pH of the photocatalytic system. Indeed, Harriman and co-workers found that the rate of O_2 evolution is optimal at pH $\sim$ 5 and decreases below and above this value.[8]

Hara et al. investigated several buffer candidates and found that both the photosensitizer decomposition rate and the turnover number depended sensitively on the composition of the buffer.[82] For a $KH_2PO_4/Na_2B_4O_7$ buffer, the turnover number depended significantly on the buffer concentration, reaching a maximum at 0.011 M. Further experiments in which $[Ru(bpy)_3]^{2+}$ was irradiated in the presence of $S_2O_8^{2-}$ and absence of IrO_2 showed that $[Ru(bpy)_3]^{3+}$ is rapidly decomposed at higher buffer concentrations. Similar experiments using either KH_2PO_4 or $Na_2B_4O_7$ showed that the culprit was the KH_2PO_4 component of the buffer. Subsequent studies focused on buffers that contain only weakly coordinating inorganic anions, such as $Na_2SiF_6/Na_2B_4O_7$ and $Na_2SiF_6/NaHCO_3$. The latter showed a sensitizer turnover

number of 290 as compared with 100 for the former, as well as a higher average rate of oxygen evolution. After $\sim$30 min, the O_2 evolution plateaus because of complete consumption of the $S_2O_8^{2-}$ sacrificial acceptor. By the addition of more $S_2O_8^{2-}$ and more HCO_3^- to bring the pH from 5.0 to 5.4, O_2 evolution resumes upon photolysis, albeit with a lower yield and lower initial rate. The lower rate of the second photolysis was ascribed to $\sim$50% decomposition of the sensitizer during the initial photolysis.

Several attempts were made to determine why bicarbonate gave a superior performance relative to borate. Both buffers were effective at maintaining the pH above 5 during the entirety of the photolysis, and both gave similar $[Ru(bpy)_3]^{2+}$ observed rate constants for decomposition in the absence of IrO_2.[82] In addition, the rates during the initial 20 min of the photolysis were similar for both buffers. The latter finding argues that the enhancement is not a result of bicarbonate-induced acceleration of reactions (10d) and (10e). Because the IrO_2 colloid is negatively charged at pH > 2,[78,80] the buffers may be influencing favorable adsorption of $[Ru(bpy)_3]^{2+}$. However, surface coverages of $[Ru(bpy)_3]^{2+}$ on IrO_2/(4-aminobutyl)dimethylmethoxysilane/SiO_2 were similar in the presence of both buffers, suggesting that the buffers do not significantly influence sensitizer adsorption.

From the above studies, it was concluded that decomposition of $[Ru(bpy)_3]^{3+}$ prevents achievement of turnover numbers > 290. Under photochemical conditions, a significant portion of $[Ru(bpy)_3]^{3+}$ is present in free solution because excited-state oxidation by $S_2O_8^{2-}$ is rapid.[82] $[Ru(bpy)_3]^{3+}$ molecules that are adsorbed to the IrO_2 are less susceptible to decomposition because they are more rapidly reduced by the colloid. In light of this finding, Hara et al. synthesized IrO_2 colloidal particles in the presence of Nafion, a perfluorinated anionic polyelectrolyte that contains sulfonate pendants.[86] Photolysis reactions comparing the $[Ru(bpy)_3]^{2+}/IrO_2$ colloid system (i.e., free colloid) with the Nafion-stabilized IrO_2 system were performed under identical conditions. In both systems, the initial O_2 evolution rates plateau at high $[Ru(bpy)_3]^{2+}$ concentration, resembling Langmuir adsorption isotherm behavior. For the Nafion system, this plateau begins at $\sim$2 × 10^{-4} M $[Ru(bpy)_3]^{2+}$, at which point the initial rate is $\sim$1.6 times that for the free colloid system. The highest quantum yields for the Nafion and free colloid systems were 73% and 45%, respectively. Meanwhile, the turnover number for both systems reaches a maximum and then falls off at higher $[Ru(bpy)_3]^{2+}$ concentrations, consistent with competition between O_2 evolution and sensitizer decomposition at higher $[Ru(bpy)_3]^{2+}$ concentrations. The O_2 evolution rates were also examined as a function of the incident light intensity at fixed $[Ru(bpy)_3]^{2+}$ concentration. For the free colloid system, the rate plateaus at high light intensities, suggesting limitations by $[IrO_2]$. No plateau was observed for the Nafion system, indicating that oxygen evolution is light-limited. The superior performance of the Nafion-stabilized system was tentatively attributed to Nafion-induced enhancement of $[Ru(bpy)_3]^{2+}/IrO_2$ adsorp

(73) Limburg, J.; Vrettos, J. S.; Liable-Sands, L. M.; Rheingold, A. L.; Crabtree, R. H.; Brudvig, G. W. *Science* **1999**, *283*, 1524.
(74) Limburg, J.; Vrettos, J. S.; Chen, H.; de Paula, J. C.; Crabtree, R. H.; Brudvig, G. W. *J. Am. Chem. Soc.* **2001**, *123*, 423.
(75) Yamada, H.; Siems, W. F.; Koike, T.; Hurst, J. K. *J. Am. Chem. Soc.* **2004**, *126*, 9786.
(76) Hurst, J. K. *Coord. Chem. Rev.* **2005**, *249*, 313−328.
(77) Ruettinger, W.; Dismukes, C. G. *Chem. Rev.* **1997**, *97*, 1.
(78) Kiwi, J.; Gratzel, M. *Nature* **1979**, *285*, 657.
(79) Kiwi, J.; Gratzel, M. *J. Am. Chem. Soc.* **1979**, *101*, 7214.
(80) Harriman, A.; Thomas, J. M.; Millward, G. R. *New J. Chem.* **1987**, *11*, 757.
(81) Harriman, A.; Pickering, I. J.; Thomas, J. M.; Christensen, P. A. *J. Chem. Soc., Faraday Trans. 1* **1988**, *84*, 2795.
(82) Hara, M.; Waraksa, C. C.; Lean, J. T.; Lewis, B. A.; Mallouk, T. E. *J. Phys. Chem. A* **2000**, *104*, 5275.
(83) Ghosh, P. K.; Brunschwig, B. S.; Chou, M.; Creutz, C.; Sutin, N. *J. Am. Chem. Soc.* **1984**, *106*, 4772.
(84) Hara, M.; Waraksa, C. C.; Lean, J. T.; Lewis, B. A.; Mallouk, T. E. *J. Phys. Chem. A* **2000**, *104*, 5275.
(85) Nahor, G. S.; Hapiot, P.; Neta, P.; Harriman, A. *J. Phys. Chem.* **1991**, *95*, 616.
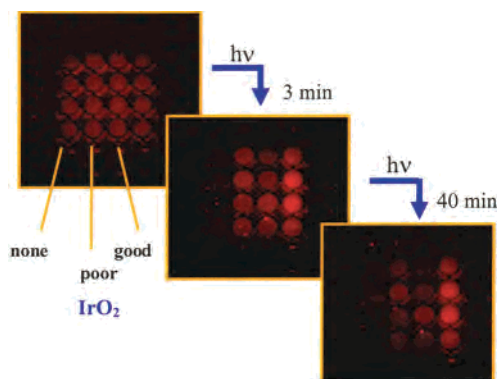(86) Hara, M.; Mallouk, T. E. *Chem. Commun.* **2000**, 1903.
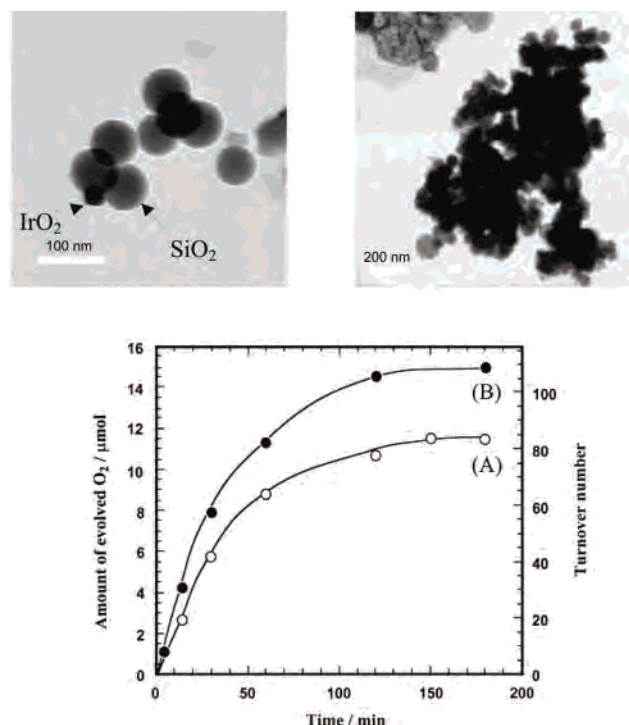
Figure 9. Top: TEM images of IrO_2/Keggin/SiO_2 and $[Ru^{2+}]_9$/IrO_2/Keggin/SiO_2. Bottom: Time course of O_2 evolution from $[Ru^{2+}]_9$−IrO_2/SiO_2 samples: (A) $[Ru^{2+}]_9$−IrO_2/SiO_2; (B) $[Ru^{2+}]_9$−colloidal IrO_2.

Figure 10. Emission snapshots of a 96-well plate containing sensitizer−colloid−sacrificial acceptor reaction solutions: lane 1, no colloid; lane 2, low activity colloid; lane 3, higher activity colloid; lane 4, no sacrificial acceptor. The emission images were acquired through a red filter by illumination with 450-nm light, after illumination of the well plate for the specified amount of time on an overhead projector. The emission signal is retained longer with better oxygen evolution catalysts.

tion, which aids in the prevention of unwanted sensitizer decomposition.

Photochemical water oxidation was further investigated using IrO_2 colloid supported on silica particles (average diameter = 70 nm).[87] By using the cationic ruthenium(II) poly(pyridyl) polymer, $[Ru^{2+}]_9$, sensitized IrO_2 containing composites (Figure 9) was made by the LBL technique. Two different multilayer sequences were studied. In the first case, anionic SiO_2 was first treated with $[Al_{13}O_4(OH)_{24}(H_2O)_{12}]^{7+}$ (Keggin) ions, followed sequentially by the IrO_2 colloid and $[Ru^{2+}]_9$. This system showed low photocatalytic activity, which was attributed to poor physical contact between $[Ru^{2+}]_9$ and the IrO_2 particles. In the second case, a solution containing $[Ru^{2+}]_9$ and IrO_2 colloid was first added to a Na_2-SiF_6/$NaHCO_3$ buffer solution, which, in turn, was immobilized on the silica support. This system showed photocatalytic activity similar to those of $[Ru^{2+}]_9$/IrO_2 colloidal solutions. Although both systems showed lower O_2 evolution rates (0.3 μmol/min) and lower turnover numbers (~90) compared to those of the optimized $[Ru(bpy)_3]^{2+}$/IrO_2 colloid system, silica-supported $[Ru^{2+}]_9$/IrO_2 does represent an integrated chemical system for photochemical oxygen evolution, which could, in principle, be coupled to a microheterogeneous hydrogen-evolving photosystem.

The problem of coupling hydrogen- and oxygen-evolving photocatalytic systems for an overall water splitting requires them to function under the same conditions (pH, buffer composition, etc.). Efficient water splitting would also require catalysts that turn over fast enough to compete kinetically with back-electron-transfer reactions. To optimize the turn-over rate of colloidal IrO_2 catalysts and rapidly explore their behavior under different conditions, we developed a simple high-throughput screening method. The method is based on the retention of $[Ru(bpy)_3]^{2+}$ absorbance or emission under continuous photolysis in IrO_2/persulfate solutions.[88] Because the destruction of the sensitizer by nucleophilic attack on the Ru(III) complex competes kinetically with catalytic oxygen evolution in cycle (10), better catalysts or better catalytic conditions correspond to longer retention of $[Ru(bpy)_3]^{2+}$ spectral properties. Figure 10 illustrates the screening method, which utilizes standard 96-well plates and a conventional plate reader. Interestingly, in a Na_2SiF_6/$NaHCO_3$ buffer, we found higher turnover numbers at higher pH (pH $\geq$ 7.0). At this pH, the SiF_6^{2-} ion is slowly hydrolyzed to colloidal silica and the system begins to resemble the microheterogeneous sensitizer/colloidal catalyst/silica system shown in Figure 9. Direct measurements of the Ru(III) lifetime in this medium show that the decomposition rate of the oxidized sensitizer is actually lower at higher pH, probably because of the interaction of the $[Ru(bpy)_3]^{3+/2+}$ complex with the anionic silica surface.

Determining the rate-limiting step in the photocatalytic cycle (10) is an essential step toward answering the question of whether colloidal IrO_2 catalysts could be useful for overall photocatalytic water splitting. For instance, if the slow step is electron transfer between $[Ru(bpy)_3]^{3+}$ and IrO_2 colloid, then the strategy for enhancing O_2 evolution rates would be to improve the electronic coupling or to increase the driving force of the reaction by changing the ligands of the sensitizer. However, if the rate-determining step is O−O bond formation or M−O bond dissociation, then it would be beneficial to redesign the catalyst itself. With this goal is mind, we performed time-resolved UV−vis spectrophotometry experiments, in which $[Ru(bpy)_3]^{3+}$ is reduced by IrO_2 colloid, and photochemical steady-state O_2 evolution studies in both H_2O and D_2O.[89] In both sets of experiments, we observed a kinetic isotope effect (KIE) of 1.0, which contrasts with the KIEs

(87) Hara, M.; Lean, J. T.; Mallouk, T. E. *Chem. Mater.* **2001**, *13*, 4668.

(88) Morris, N. D.; Mallouk, T. E. *J. Am. Chem. Soc.* **2002**, *124*, 11114−11121.

of 1.4 and 1.6 reported for the molecular O_2-evolving complexes, *cis*,*cis*-[[(bpy)$_2$Ru(OH$_2$)]$_2$O]$^{4+}$ and [(terpy)(H$_2$O)-Mn^{III}(O)$_2$(OH$_2$)(terpy)]$^{3+}$, respectively. This suggests that the rate-determining step in water oxidation at IrO_2 colloids is outer-sphere electron transfer between the oxidized sensitizer and the colloid.

Time-resolved studies confirmed that the oxygen evolution reaction follows second-order kinetics and that increasing the concentration of either reagent increases the reaction rate. This finding is consistent with an earlier observation by Harriman and co-workers that the rate of water oxidation by radiolytically oxidized IrO_2 clusters is quite fast.[90] Under the conditions normally used for photocatalytic cycle (10), the steady-state concentration of photogenerated [Ru(bpy)$_3$]$^{3+}$ is low and therefore the oxygen evolution rate is low. By using relatively high concentrations of the [Ru(bpy)$_3$]$^{2+}$ sensitizer, oxidizing it photochemically to [Ru(bpy)$_3$]$^{3+}$, and then injecting the IrO_2 colloid, we were able to reach site turnover rates of about 160 s^{-1}, which corresponds to O_2 evolution at a rate of about 40 molecules per second per surface Ir atom. This result is very encouraging for the possible use of IrO_2 colloids in water-splitting systems. It also helps to explain why supports for IrO_2 such as Nafion, which is a good cation exchanger, lead to higher [Ru(bpy)$_3$]$^{3+}$ turnover rates. Such supports serve to concentrate the oxidized sensitizer at the surface of the colloid, leading to a higher rate of electron transfer.

Conclusions and Outlook

Photocatalysis lags behind other solar energy conversion methods, in particular photovoltaic and photoelectrochemical electrolysis, as a means of generating hydrogen from water. However, there is no fundamental reason that photocatalytic systems cannot be efficient. We now understand the principles of electron transfer well enough to design reasonably good systems for both the water oxidation or water reduction half-cell reactions. The problem of joining these half-cell systems together in ways that prevent electron−hole and chemical product recombination reactions remains the most important challenge in achieving an efficient overall water splitting with visible light.

IC050779J

(89) Morris, N. D.; Suzuki, M.; Mallouk, T. E. *J. Phys. Chem. A* **2004**, *108*, 9115.
(90) Nahor, G. S.; Hapiot, P.; Neta, P.; Harriman, A. *J. Phys. Chem.* **1991**, *95*, 616.